ARTICLE

Check for updates

Seasonal stratification and complex local dynamics control the sub-surface structure of marine heatwaves in Eastern Australian coastal waters

Amandine Schaeffer [1,2✉], Alex Sen Gupta [2,3] & Moninya Roughan [2,4]

Marine heatwaves are extreme seawater temperature events that can have severe impacts on marine life. The extent of the ecological damage depends not only on the easily observed surface signature but on the marine heatwave structure at depth. However, due to a paucity of in situ sub-surface observations the vertical structure of marine heatwaves is poorly understood. Here we analyse the sub-surface coherence and controls of marine heatwaves using one of the world's longest (28 years) records of daily sub-surface ocean temperature off Sydney, Australia. We show that seasonal stratification, large-scale circulation and local downwelling processes control the vertical coherence of coastal marine heatwaves. We define three classes of marine heatwaves which can extend through the water column, form in the shallow surface layer, or sub-surface independently, and are therefore not always evident in surface data. We conclude that sub-surface data need to be considered in monitoring marine heatwaves in coastal areas where maximum biological damage is reported.

[1] School of Mathematics and Statistics, UNSW Sydney, Sydney, Australia. [2] Center for Marine Science and Innovation, UNSW Sydney, Sydney, Australia. [3] Climate Change Research Center, UNSW Sydney, Sydney, Australia. [4] School of Biological, Earth and Environmental Sciences, UNSW Sydney, Sydney, Australia. ✉email: a.schaeffer@unsw.edu.au

Ocean temperature extremes, and in particular marine heatwaves (MHWs) are a growing concern in the science community and across fisheries and tourism industries. There has been a large increase in their frequency, duration and intensity across recent decades[1], primarily due to long-term ocean warming[2], which are projected to accelerate in the future[3–5]. Widespread impacts have affected many regions and diverse marine ecosystems[6].

Despite recent advances in the understanding of the characteristics, drivers, and impacts of MHWs, monitoring and characterising extremes below the ocean surface is a challenge[7,8]. MHWs are commonly defined as periods of particularly intense temperature anomalies, relative to some threshold (e.g. a daily varying 90th percentile[9]). To construct a robust threshold that can capture the full range of MHW timescales requires high-frequency observations over a number of decades (e.g. 3 decades[9,10]). However, while satellite measurements provide daily SST going back to the early 1980s, making it possible to identify heatwaves at the surface for most parts of the global ocean, few in situ platforms have been consistently measuring ocean temperature below the surface for sufficient duration to define a robust baseline climatology. Therefore, most knowledge of MHWs is derived from surface observations and modelling outputs, and little is known about the occurrence or coherence of events at depth.

Few studies have systematically looked at sub-surface MHWs, and even fewer have provided directly in situ insight into the depth structure of MHWs rather than being derived from model outputs. Importantly, a typical recurrent sub-surface maximum for the intensity of MHWs was observed in coastal areas off Sydney[11] and in the open ocean in the tropical Western Pacific[12]. Off the eastern Australian continental shelf, ARGO floats were used to show that temperature anomalies can extend down to 2000 m during some surface-identified MHWs, in particular in winter within anticyclonic warm-core eddies[13], that have deep mixed layers[14]. Follow-up modelling work was able to link the drivers of MHWs in the surface mixed layer to their depth extent, showing that regional MHWs driven by anomalous advection are on average three times deeper than those driven by surface air–sea heatfluxes[15]. In addition to these MHW events that extend deep, there are also sub-surface events that do not have an unusually warm surface signature, as observed by Schaeffer and Roughan[11], Hu et al.[12], Scannell et al.[16] and modelled by Grosselindemann et al.[17] and Amaya et al.[18]. These events would affect benthic communities while being undetected at the surface.

Marine heatwaves that occur on the continental shelves are of particular importance, as these regions host most fisheries and tourism enterprises. Some individual events have caused massive financial losses to regional industries[19] and their frequency has increased, as shown from rare long-term monitoring sites, e.g. in New Zealand[20], and on the Finish shelf, reaching the bottom in 30 m water depth[21].

Continental shelf regions are subject to unique dynamical processes due to the shallow depths and proximity to land. Previous work has shown that MHWs along the coast can often occur independently of large-scale, off-shelf events, even at the surface[20–22]. The local oceanographic conditions and associated temperature variability on the continental shelf off southeast Australia are strongly modulated by the intrusion of large-scale currents[23,24] and atmospheric conditions. The large-scale ocean circulation is dominated by the southward-flowing East Australian Current (EAC) Western Boundary Current, and its eddies[25], which advect warm water from the tropics to subtropics (Fig. 1e), extending to depths >400 m (considering a mean along-slope speed that exceeds 0.2 m s^{-1})[26].

The prevailing southerly winds are downwelling favourable[27,28], but intermittent northerly winds trigger cold water upwelling[29]. Compared to the atmosphere, the seasonal cycle in ocean temperature is delayed, with a maximum stratification in February and a minimum in July.

In this study, we use a unique 28-year (1992–2019) in-situ record of daily temperatures through the water column on the southeast Australian shelf to examine the characteristics and drivers of synchronous and asynchronous surface and sub-surface MHWs. We use a commonly used framework to identify MHWs relative to a seasonally varying 90th percentile threshold using high-frequency measurements at all depths from the surface to 53 m from a sustainable moored platform (Fig. 1a, ORS065 mooring site, depth of 65 m). This is complemented by satellite sea surface temperature (SST) and local observations of ocean currents and meteorological conditions.

As shown by Schaeffer and Roughan[11], winds and stratification impact the depth-structure of MHWs in the area. Here, we expand on this work and define an MHW categorisation according to their vertical structure. In particular, MHWs may be (i) *shallow* (that are confined to the surface layer not deeper than a threshold, here 35 m), (ii) *extended* (that extends deeper and potentially through the full water column), and (iii) *sub-surface* (that are deep, here close to the bottom, but have no surface signature). We assess the drivers of these different MHW types and discuss the link with the mixed layer depth. We investigate if information about the sub-surface structure of MHWs can be inferred from satellite sea surface temperature (SST) depending on the seasonal stratification, and determine how the inter-annual variability in the occurrence of MHWs is related to large-scale atmospheric and ocean conditions.

Moving forward, our results suggest a means for predicting the presence of sub-surface temperature extremes based on a knowledge of the background ocean and atmosphere conditions in locations where sustained sub-surface observations are unavailable.

Results

Contrasting *shallow*, *extended*, and *sub-surface* MHWs. Observational evidence of MHWs that span the whole water-column is rare because of the lack of sub-surface data. Most MHWs described in the literature are *shallow*, restricted to the shallow surface mixed layers in summer months, like the event at the mooring location in December 2000 (Fig. 1b). Figure 1c shows that both the satellite SST (based on the nearest grid cell) and in situ measurements from the ORS065 mooring site, identify a strong to moderate MHW. The MHW extends from the surface to 35 m based on the definition from ref. [9], but fades away below this. We refer to these events as *shallow* MHWs. At that time, SST anomalies were elevated over a broad domain, with no indication of an enhanced geostrophic current affecting the mooring site (Fig. 1b).

There are, however, times when MHWs span the whole water-column, extending deep, which we refer to as *extended* MHWs. For instance, an MHW that peaked around the 27th of July 2001 was evident at each depth level in either the moderate or strong category (Fig. 1d, following a classic definition[30]), including at the surface based on satellite SST. The spatial map (Fig. 1e) shows a southward flow along the coast associated with warm anomalies, suggesting that warm water from the EAC is being brought on-shelf, thereby providing conditions for the MHW.

Finally, the most problematic events to detect are those with no surface expression, where the temperature is only extreme in the sub-surface. We refer to these events as *sub-surface* MHWs. An
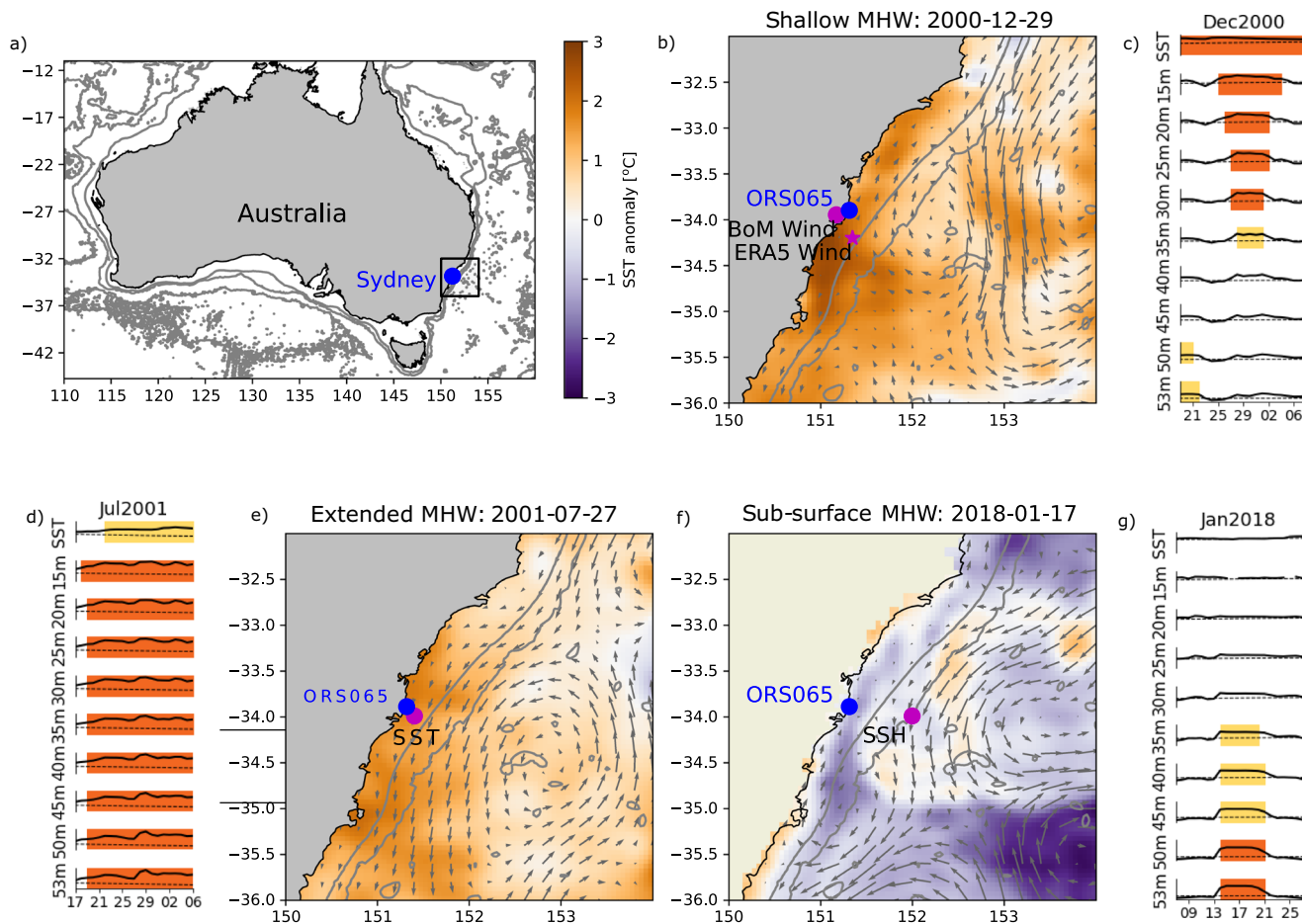
Fig. 1 Example of *shallow*, *extended*, and *sub-surface* MHWs. a Area of interest (black box); Satellite SST anomalies and ocean geostrophic velocity vectors (black arrows) during, **b** a *shallow* MHW (2000-12-29), **e** an *extended* MHW (2001-07-27), **f** a *sub-surface* MHW (2018-01-17). The blue dot in each panel indicates the location of ORS065 mooring. The wind station (BoM wind), location for ERA5 wind estimates, satellite SST, and satellite geostrophic currents (SSH) used in the subsequent analysis are indicated by magenta symbols. The 200 and 1000 m isobaths are shown in grey. For each date, the temporal evolution of temperature (solid-line) compared to the climatology (dashed line) over 20 days (centred on the MHW event) is shown from satellite SST (top) and ORS065 mooring (depths 15–53 m) in panels **c**, **d**, **g** with respective y-axis range 15–25, 16–21, and 15-25 °C. Yellow and orange shadings indicate moderate and strong MHW, respectively.

example is shown in Fig. 1g (January 2018), where the temperature above 35 m depth was not warmer than the 90th percentile. In this case, the surface map indicates a cold surface anomaly, across a broad area and a weak circulation on the shelf (Fig. 1f). As such, the event would not have been picked up if in situ mooring data were not available.

Overall, during the 28 years of ORS065 mooring data, we identified 17 *shallow* events, 16 *sub-surface* events and 19 *extended* events following a conservative definition (see section "Methods"). All the events are shown in Fig. 2, together with the temporal evolution of the smoothed surface mixed layer depth. The following sections investigate their characteristics and drivers.

Characteristics of *shallow*, *extended*, and *sub-surface* MHWs. *Shallow* and *sub-surface* MHWs occur most frequently in strongly stratified months from January to March (7 and 10 events, respectively, Fig. 3a, e) with no *shallow* and only two *sub-surface* events in weakly stratified months (July–September). In contrast, *extended* events are the most frequent during the weak seasonal stratification from July to September (Fig. 3c, 8 events) although they are more evenly distributed over the year than *shallow* and *sub-surface* events.

Overall, there is weak and very strong evidence that *surface* and *subsurface* events, respectively, are more frequent in January–March compared to other 3-month periods (one-sided z-test, with the null hypothesis that each 3-month period has an expected proportion of 1/4; $n = 17$, $z^* = 1.36$, and p-value $= 0.09$ for *surface* events; $n = 16$, $z^* = 3.10$, and p-value $= 0.00097$ for *sub-surface* events). There is weak evidence that *extended* events are more frequent in July–September compared to other 3-month periods ($n = 19$; $z^* = 1.51$, and p-value $= 0.066$).

The longest MHWs tend to be the *extended* events (median and mean duration of 11 and 14 days, (Fig. 3d) while *sub-surface* events are typically the shortest and the most intense with mean and median duration and intensity of 7 days and 3.3–3.1 °C (Fig. 3f). This is in agreement with findings from ref. [11], which show the greatest temperature variance around 53 m, hence more potential for elevated MHW intensities.

Drivers of *shallow*, *extended*, and *sub-surface* MHWs. Several observed atmospheric and ocean variables are known to impact the ocean heat budget. Wind speed affects vertical mixing, latent and sensible heat fluxes, while persistent alongshore winds generate upwelling (when blowing from the north) and downwelling (when blowing from the south). Reduced cloud cover (often
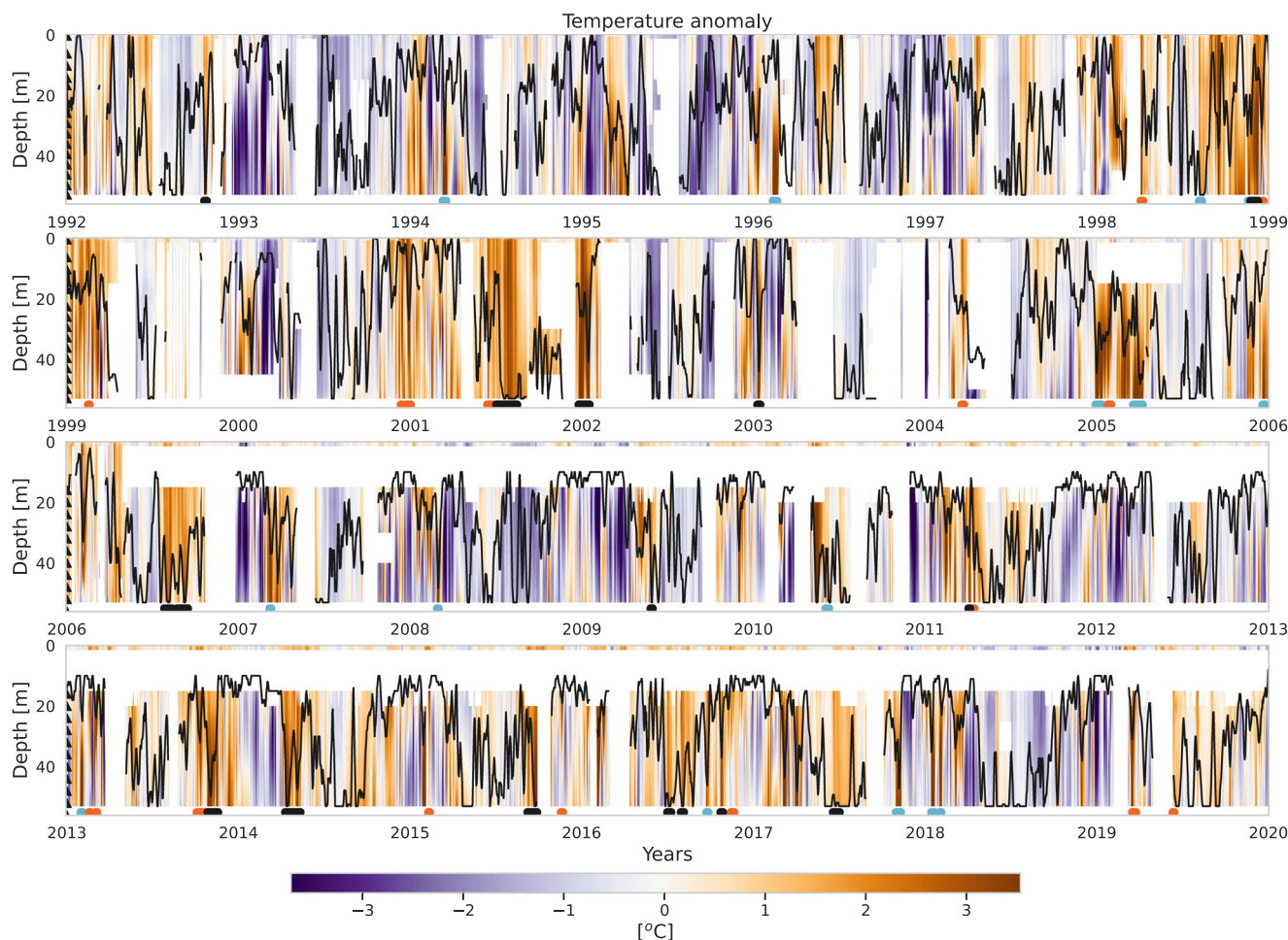
Fig. 2 De-seasonalised temperature anomalies over time. The surface data comes from satellite SST while sub-surface measurements are from the in situ ORS065 mooring. Note the missing surface coverage of the mooring after 2006 (hence MHWs were not detected between 0 and 15 m). The timing of the *shallow*, *extended*, and *sub-surface* MHW events are indicated at the bottom of the panels by red, black, and cyan symbols, respectively. The mixed layer depth smoothed over 5 days is indicated (defined as the shallowest depth where the temperature exceeds the SST temperature by more than 0.5 °C[40]) as salinity is not measured in the water column and has a negligible effect in the region overall[23,29]). Black triangles on the left of the panels show the depth of instruments which changed in 2006.

associated with high air temperature) increase short-wave radiative heat-fluxes. In the ocean, advection of heat typically comes from a strong EAC and associated eddies that advect warm tropical waters southwards (for example, see Fig. 1e). In addition, local near-shore circulation can also affect temperature. To examine the various drivers of temperature extremes at the mooring site, we analyse wind and air temperature measurements from a close-by land-based weather station (location shown in Fig. 1b) and extract air–sea heat-fluxes from the ERA5 atmospheric reanalysis[31,32]. We use satellite observations of the large-scale geostrophic ocean currents and depth-integrated in situ local currents measurements at ORS065 as proxies for the large-scale and local ocean circulation, respectively.

Using anomalous variables, averaged over the build-up phase of each event (defined as the 7 days before each MHW peak), we relate the events to atmospheric or ocean drivers. *Extended* MHW events mostly peak following anomalous southward geostrophic ocean currents (median of −0.5 standard deviations from the mean, Fig. 4c), which suggests the influence of an anomalous EAC intruding the continental shelf and advecting the heat over the whole water-column. Other normalised variables are scattered around zero, with no consistent anomaly prior to the MHW events (Fig. 4c). Reanalysed air–sea heat-fluxes indicate an

anomalous cooling of the ocean during the MHW buildup associated with air–sea fluxes predominantly from enhanced latent heat-fluxes (Fig. 4d).

Sub-surface MHW events tend to peak following northward local current anomalies on the shelf (normalised median of 0.9, Fig. 4e, but note the low number of events due to limited data availability). This local along-shelf current is likely resulting from the northward (downwelling-favourable) wind stress anomalies (normalised median of 0.7) with increased wind speed (normalised median of 0.6) (Fig. 4e). Hence, the sub-surface warming appears to result from the deepened thermocline associated with the downwelling-favourable winds. The larger scale ERA5 winds also indicate the same northward anomaly (Fig. 4f, 2.3 m s^{-1} which corresponds to a normalised value of 0.5 standard deviations above the mean). Interestingly, all air–sea heat-fluxes (except long-wave) show negative anomalies, indicating enhanced ocean heat loss at the surface during *sub-surface* MHW events. The net heat loss is predominantly driven by the latent heat fluxes with an average anomaly of 39.3 W m^{-2}. This is consistent with the increased wind speed during the build-up of the *sub-surface* MHW events.

The only MHW events that are typically driven, at least in part, by air–sea heat fluxes are the *shallow* events, for which local winds
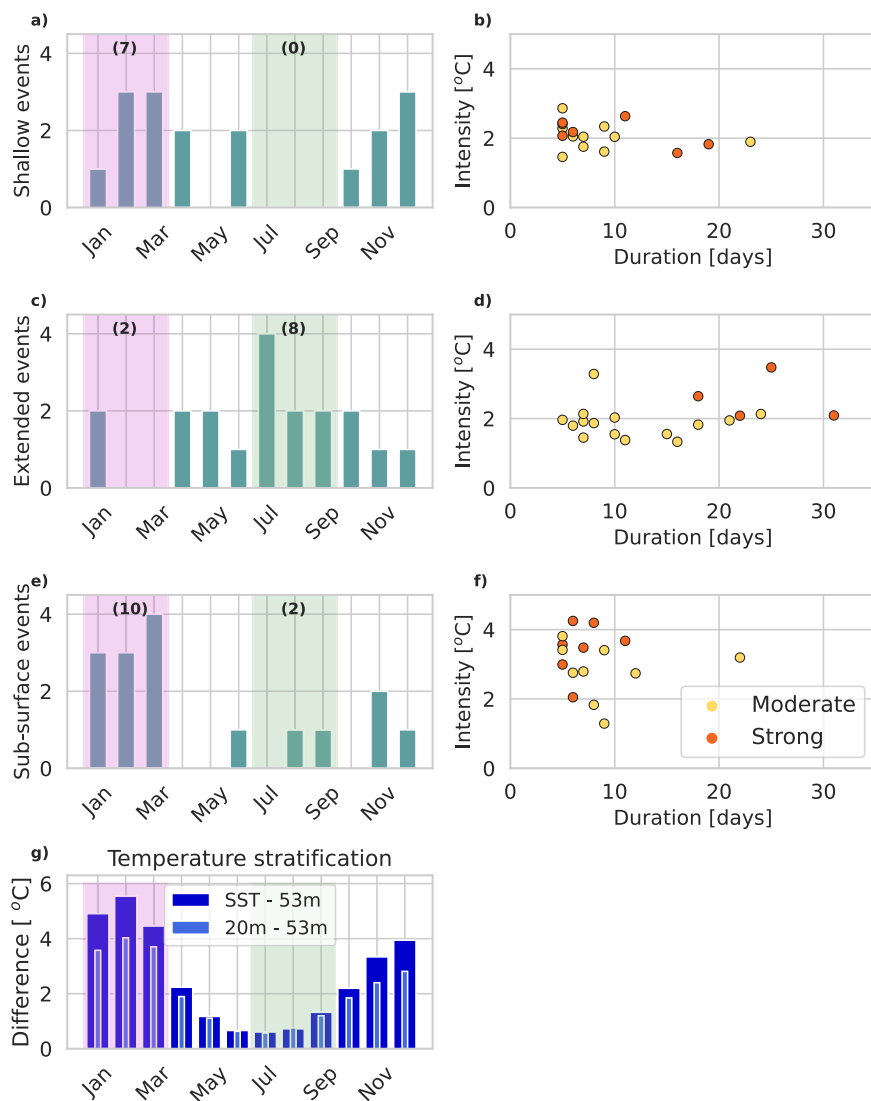
Fig. 3 Characteristics of *shallow*, *extended*, and *sub-surface* MHWs. Monthly occurrence and characteristics (mean events intensity and duration) of *shallow* (**a**, **b**), *extended* (**c**, **d**), and *sub-surface* (**e**, **f**) MHW events. Events in **b**, **d**, **f** are colour-coded based on their intensity category (moderate or strong). Monthly mean stratification is shown by the difference between temperature close to the surface and bottom (**g**). Purple and green shadings highlight the strongly and weakly stratified months, respectively, with the number of MHW events indicated in brackets.

and currents show little consistency (Fig. 4a). The net heat-fluxes anomalies are generally positive, mostly related to increases in short-wave radiation (anomaly of $14.7\,\mathrm{W\,m^{-2}}$, Fig. 4b), which suggests a reduced cloud coverage, in agreement with anomalous warm air temperature (Fig. 4a).

SST as a proxy for daily MHWs below the surface. In the previous section, we show that *extended* MHW events mostly occur during the weakly stratified months, and appear to be driven by large-scale advection. Here we address the question of when SST is a good proxy for deep MHWs, looking at similarities in the timing of MHWs in the sub-surface compared to the days identified as MHWs in the satellite SST dataset.

We define the 'coherence' as the percentage of the total number of MHW days at the surface (using satellite observations) that are also MHWs at different depths (Fig. 5b; the total number of surface MHW days is shown in the legend). Note that each depth is compared to the surface, independently of other depths (hence there is not necessarily a vertical continuity). Also, these proportions, reaching a maximum of 57%, are likely an underestimate due to the small discrepancies between the satellite SST

and the in-situ measurements[33], shown in Supplementary Fig. S1. The satellite product is representative of larger areas and may have accuracy issues related to factors such as cloud cover. Small-scale deviations in temperature within the satellite footprint can also arise from small-scale dynamics[22].

During weakly stratified months, defined as JAS (July–August–September, 6 months after the strong JFM January–February–March stratification (Fig. 3g) the mean temperature profile is relatively homogeneous with depth (Fig. 5a) and MHWs are typically coherent with depth (green line in Fig. 5b). Between 43% and 57% of surface MHW days co-occur with MHWs days which were identified in the different depth layers between 15 and 53 m. In contrast during strong stratification months, the mean temperature drops from 23 °C at the surface to 17 °C at 53 m (Fig. 5a) and the coherence also drops rapidly with depth (purple line in Fig. 5b). Indeed, the co-occurrence between surface SST MHW days and deep MHW days is only 6% at 53 m depth. This means that in strongly stratified months, out of the 218 MHWs days identified from satellite SST, only 13 days are also in MHW condition at 53 m depth.
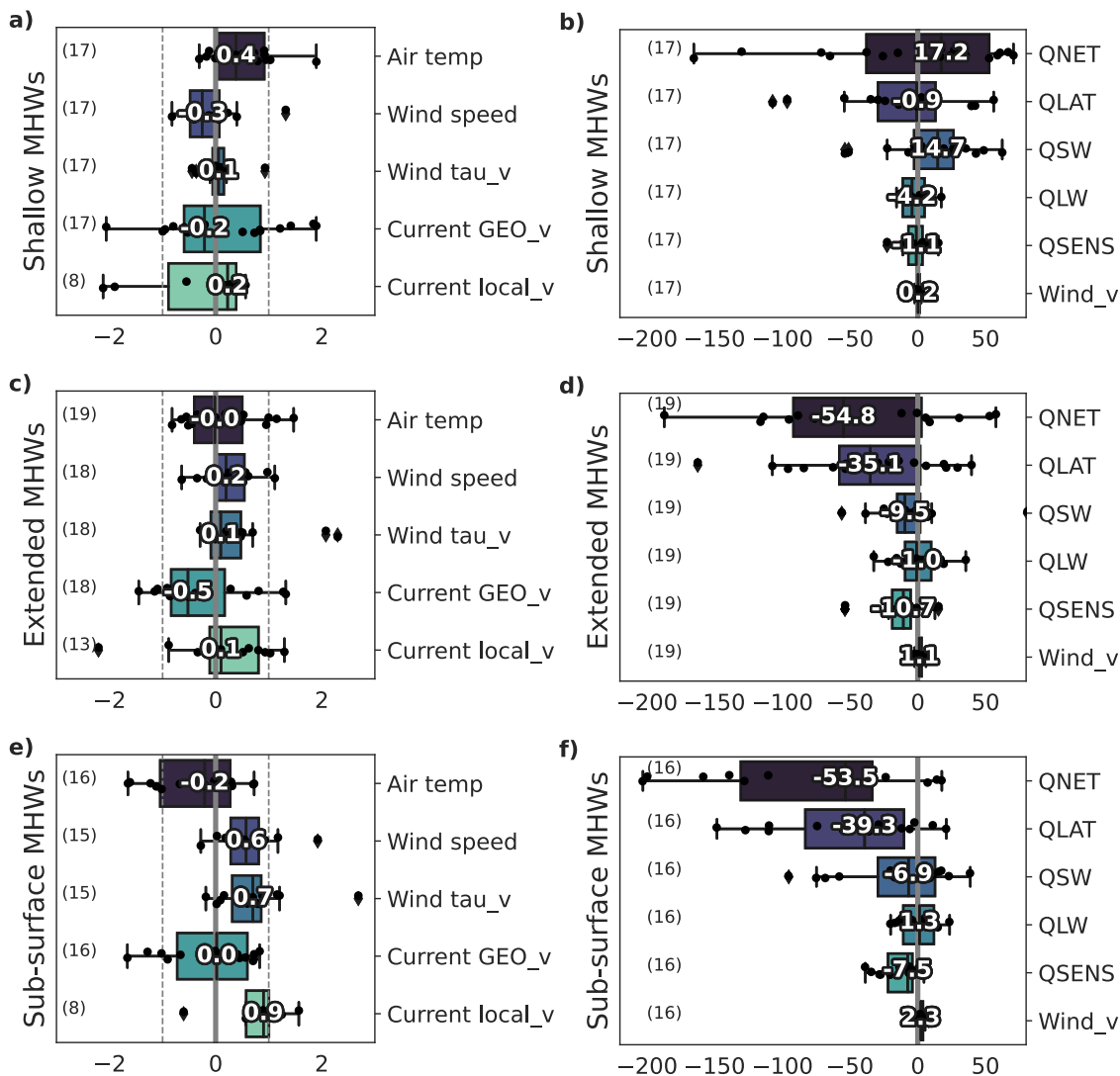
Fig. 4 Anomalous conditions during the onset of *shallow, extended,* and *sub-surface* MHWs. Box-plot of anomalous conditions averaged over the onset (7 days before the peak) of each *shallow* (**a**, **b**), *extended* (**c**, **d**) and *sub-surface* (**e**, **f**) MHW event. Left panels show the observed normalised (by the seasonal standard deviation) anomalies of 2 m-air temperature, wind speed, meridional wind stress (Wind tau_v), geostrophic meridional current velocity (Current GEO_v), and depth-integrated local meridional current velocity (Current local_v). Right panels show anomalies from ERA5 reanalysis: net (QNET), latent (QLAT), short-wave (QSW), long-wave (QLW) and sensible (QSENS) heat-fluxes (in W m^{-2}), and meridional wind velocity (Wind_v in m s^{-1}). Note that positive anomalies for meridional velocities indicate a northward anomaly, and for heat-fluxes indicate heat into the ocean. The boxes show the quartiles of the dataset while the whiskers show the lowest (highest) data points still within the 1.5 inter-quartile range of the lower (upper) quartile and the median values are shown in white. The number of events is indicated in brackets and individual events are shown with circles.

Figure 5 also subsets the events by northward versus southwards geostrophic current anomalies. Compared to stratification, the direction of the current has a relatively small impact on the coherence of the MHW with depth. Common MHW days with SST vary by <13% between periods when the geostrophic current anomaly is positive (northward) or negative (southward). The direction of the large-scale advection does however modulate the number of surface MHWs. A majority of MHW days at the surface (72%, 120 of 172) occurred during anomalous southward flow during weakly stratified months, which contrasts with a 50/50 ratio of southward/northward anomalies during strong seasonal stratification.

SST as a proxy for inter-annual MHW days below the surface. Given the fact that MHWs tend to be more coherent with depth in weakly stratified periods, we might also expect inter-annual variability of MHW occurrence to be the most coherent with

depth during periods of weak seasonal stratification, providing some level of proxy or predictability for deep extreme events.

The number of surface MHW days in JAS (weak stratification) each year based on satellite SST at the mooring location is remarkably representative of the sub-surface MHW variability (Fig. 6a). Correlation coefficients between surface (satellite SST) and deep (in situ) time-series range between 0.80 and 0.86 across the water column over the 1992–2019 period (Fig. 6b). In contrast, during JFM (strong stratification), correlation coefficients are strong near the surface layer (0.78 between SST and 20 m depth temperature), but much lower (<0.26) for depths >30 m (Fig. 7b). Some years were characterised by a high number of MHWs in JFM (stratified months) only at the surface, e.g. 2001 or 2013, while other years had MHWs mostly at depths > 20–25 m, e.g. 2005 (Fig. 7a).

To investigate the drivers of these interannual variations, we examine the link between seasonal MHW day counts each year as
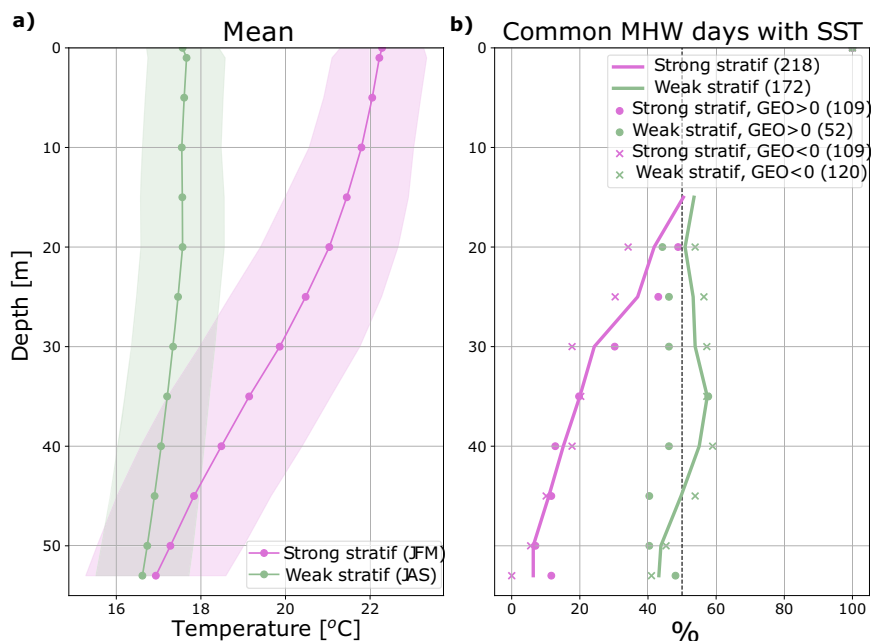
Fig. 5 Seasonal mean temperature and coherence of MHWs over depth. Depth-profile of **a** mean temperature and **b** MHW coherence: percentage of MHW days at the surface (from satellite data) which co-occur with an MHW at depth (from in situ measurements). Purple and green colours correspond to strongly stratified (JFM) and weakly stratified periods (JAS), respectively. The dots and stars in **b** show the coherence during positive (northward) and negative (southward) geostrophic current anomalies, respectively. The total number of SST MHW days for each category is indicated in brackets. Note that **a** includes the top layer (1–10 m depth) which was only sampled before 2006.

a function of depths and corresponding ocean and atmospheric seasonally averaged anomalies. In weakly stratified months, the total number of MHW days is significantly negatively correlated with the meridional component of the geostrophic current velocity at all depths (Fig. 6f, correlation around −0.4). This is clear in the time series (Fig. 6e), where peaks in MHW days match southward current anomalies, e.g. in 1998, 2001, 2006, 2015–2016.

We found some counter-intuitive relationships that were statistically significant in Fig. 6g, h, e.g. MHW days counts and reduced short-wave radiation at the surface, or MHW day counts and decreased latent heat fluxes in ERA5 reanalysis. These may be spurious relationships related to data issues or might result from some additional process affecting both of the variables.

In strongly stratified months, the greatest association is found between sub-surface MHW day counts and increased heat loss from latent heat-fluxes (Fig. 7h, negative correlations), increased northward wind component, and wind speed (Fig. 7c, d). Hence, stratified months with anomalously strong downwelling-favourable winds have more MHWs days below 30 m, which is consistent with drivers for individual *sub-surface* MHW events in the previous section. However, in the surface layers, the strongest relationships are between MHW days and heat loss from latent heat-fluxes (Fig. 7h), in contrast with our analysis for individual events which identified short-wave fluxes anomalies in the build-up of *shallow* events as being important.

Discussion

This rare dataset provides new observational insights into the depth structure and characteristics of MHWs throughout the water column. Our results facilitate a robust classification of MHWs based on their depth extent.

The three categories and their driving mechanisms are summarised in Fig. 8. Both *surface* and *sub-surface* MHWs occur during stratified months whereas *extended* MHWs are dominant during well-mixed periods. In our study site, stratification and

mixing are seasonal and modulated by prevailing winds and currents.

Shallow MHWs (Fig. 8 left) occur mostly during seasonally stratified months and are typically associated with positive air–sea heat flux anomalies, primarily related to increased insolation (reduced cloud coverage). *Sub-surface* MHWs (Fig. 8 right) can be more challenging to identify and predict since they are not discernible from the surface. They typically occur in response to intensified downwelling favourable winds, which also enhance surface mixing and cooling by turbulent heat fluxes of surface waters, amplifying the decoupling of temperature anomalies between the surface and deeper in the water column. Note that the decoupling would not occur with suppressed upwelling winds, which also impact temperature anomalies in the sub-surface[34]. We find that *sub-surface* MHWs are generally not as long-lasting as surface events, but are the most intense. Their potential for predictability is linked to the predictability of downwelling favourable wind conditions.

Extended MHWs (Fig. 8 bottom), which span most of the shelf water column simultaneously are the longest, and often associated with anomalous large-scale ocean circulation, e.g. intrusion of the EAC.

These results are consistent with previous studies. In the tropical western Pacific Ocean[12], analysed MHWs from 19 buoys down to 500 m, which recorded high-frequency temperatures since the 1990s. They considered that most of the events were sub-surface based on the deep maximum intensity (which would correspond to our categories *extended* and *sub-surface*), and related them to Ekman downwelling and surface convergence of currents. Focusing on the depth structure of MHWs in the Gulf Stream region, a modelling study[17] focused on two contrasting case studies. The surface (shallow) MHW was driven by air–sea heat-flux, and the deep MHW was caused by the intrusion of a warm core ring onto the shelf. Other modelling results[18] did not consider driving mechanisms but also highlighted the recurrent lack of synchronicity between surface and bottom MHWs, in
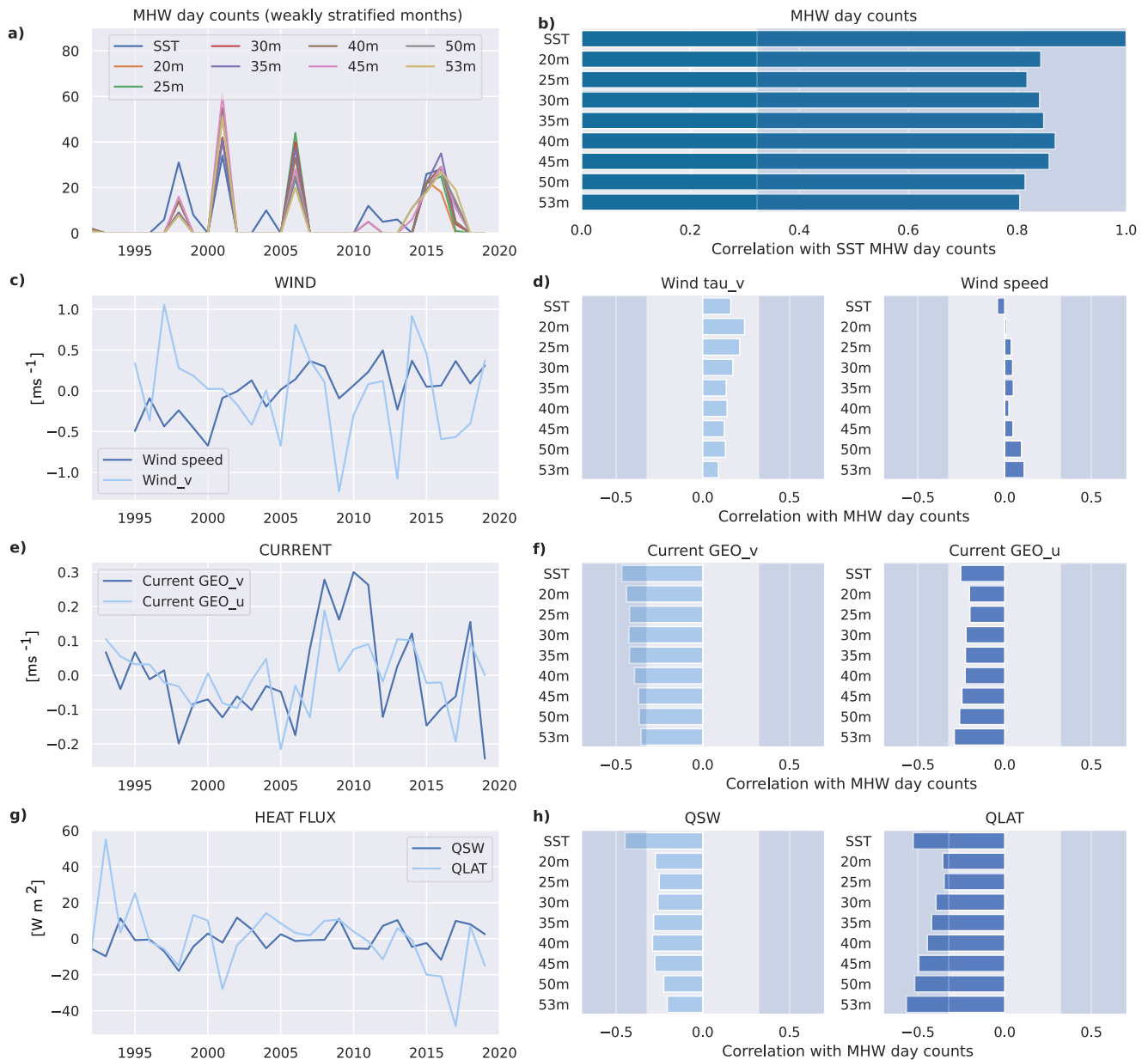
Fig. 6 Inter-annual variability of MHW day counts and other variables during weakly stratified months. Annual time-series (left panels) and Pearson correlation coefficients with annual MHW day counts at different depths (right panels) in weakly stratified periods (JAS) for **a**, **b** SST MHW day counts, **c**, **d** observed wind speed and meriodional component anomalies, **e**, **f** satellite geostrophic meridional and zonal current velocity anomalies, **g**, **h** short-wave and latent heat flux anomalies from ERA5. For instance, in panel **h**, the bar at depth "40 m" for panel QSW shows a Pearson correlation between the MHW days count at 40 m (shown in brown in panel **a**) and the short-wave heat-flux anomalies (shown in dark blue in panel **g**) over the 1995–2019 period (25 data points). Shaded correlation magnitudes > 0.32 are significant at < 0.1 level for 25 degrees of freedom (assuming each year is independent between 1995 and 2019 when all data is available).

particular in regions of the North American continental shelves that are deeper than the surface mixed layer.

It is clear that seasonal stratification is an important factor for MHW development, as already shown in the same region[11]. *Shallow* MHWs most commonly occur when the climatological mixed layer is shallow and surface heat fluxes warm a relatively small volume of water. But strong surface heating further stratifies the water column and shoals the mixed layer[8,34]. In some regions, a freshwater outflow that enhances stratification was also shown to inhibit the deepening of warm anomalies[16]. *Sub-surface* MHWs also tend to be most prevalent when the water column is more stratified, hence decoupled from the surface. Here, it is

predominantly downwelling favourable winds that act on larger vertical temperature gradients and enhance sub-surface warming. Unlike *surface* events, *sub-surface* events that warm below and cool above would tend to make the water column less stratified which could explain their shorter duration. The intrusion of large-scale currents such as the EAC with warm cores that can extend 100s of metres below the surface can lead to *extended* MHWs irrespective of the stratification of the water column prior to the intrusion event.

Here we characterise MHWs as *shallow*, *extended*, or *sub-surface*, based on where they lie in the water column. These would impact ecosystems at different depths. Relatively passive floating organisms
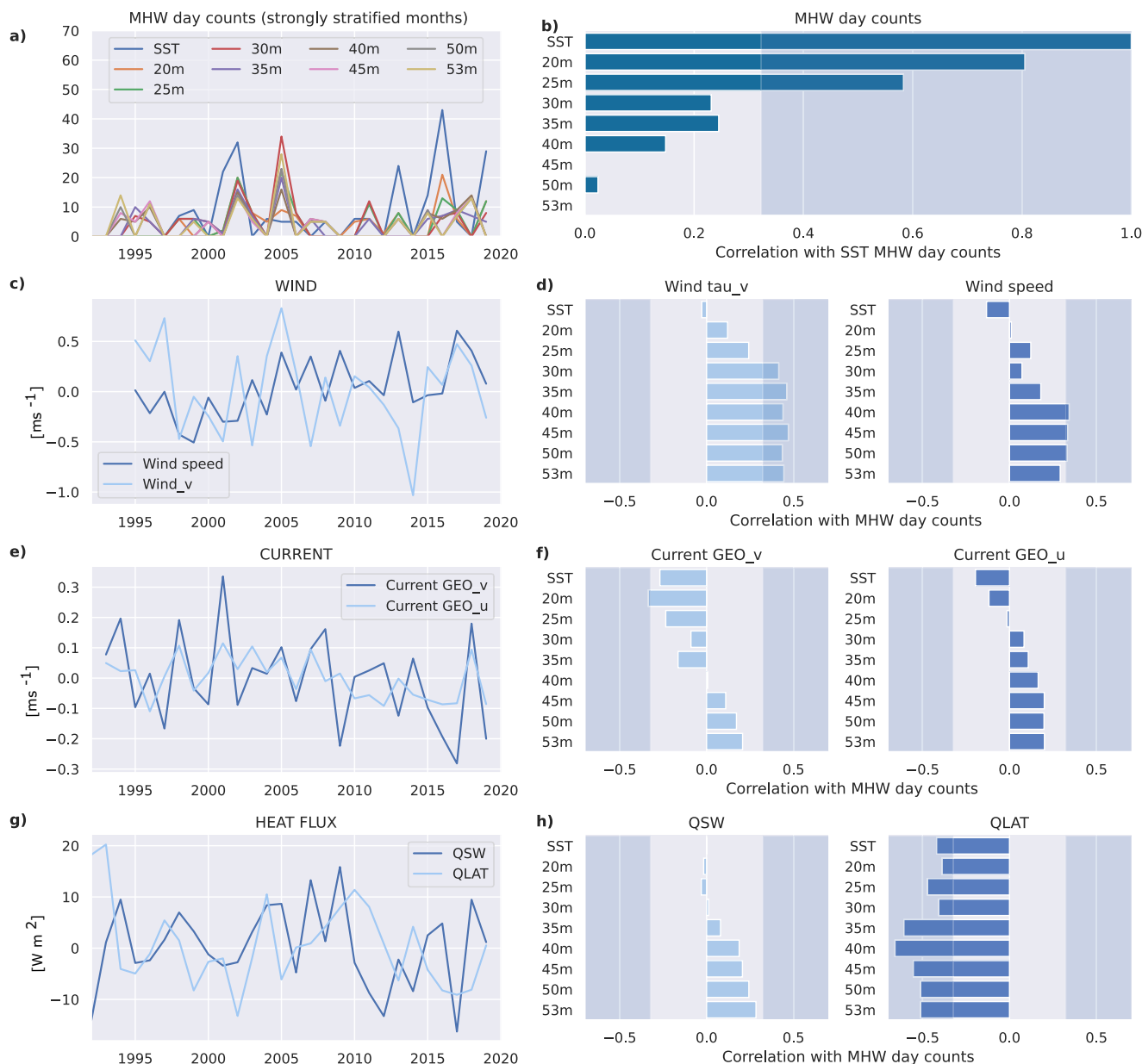
Fig. 7 Inter-annual variability of MHW day counts and other variables during strongly stratified months. Annual time-series (left panels) and Pearson correlation coefficients with annual MHW day counts at different depths (right panels) in strongly stratified periods (JFM) for **a**, **b** SST MHW day counts, **c**, **d** observed wind speed and meriodional component anomalies, **e**, **f** satellite geostrophic meridional and zonal current velocity anomalies, **g**, **h** short-wave and latent heat flux anomalies from ERA5. Shaded correlation magnitudes > 0.32 are significant at <0.1 level for 25 degrees of freedom (assuming each year is independent between 1995 and 2019 when all data is available).

would be particularly sensitive to *shallow* and *extended* MHWs, while benthic species would be affected by *sub-surface* or *extended* MHWs in coastal areas. Motile pelagic species might be able to find refuge by changing depth or moving away from the affected areas.

In conclusion, satellite-derived MHW identification is only a good proxy for deep extremes when the water column is well-mixed. Moreover, since MHWs extending through the water column are often tied to ocean heat advection anomalies, satellite geostrophic currents may be an important tool for predicting the depth-extent of MHWs.

In contrast, satellite temperature anomalies cannot reliably infer MHW conditions below the surface mixed layer during stratified periods. This is due to the dominant influence of air–sea heatfluxes in driving surface MHW which do not extend much deeper than the shallow mixed layer, and are accentuated in

coastal areas by wind forcing that can generate opposing impacts on temperature anomalies at the surface and closer to the bottom. In order to infer whether or not there are temperature extremes below the shallow surface mixed layer in stratified periods, the best proxy appears to be wind anomalies since *sub-surface* MHWs events and years characterised by many MHW days are predominantly associated with wind-driven downwelling that depresses the thermocline.

Given the drivers and prevailing conditions described at this mooring occur in other locations, it seems quite plausible that similar processes may operate in other locations. In particular, they may be more generally applicable to regions that experience regular stratification (from seasonal heating or freshwater outputs), and prevailing downwelling-favourable winds. Unfortunately, long-term sub-surface observations are rare in other locations.
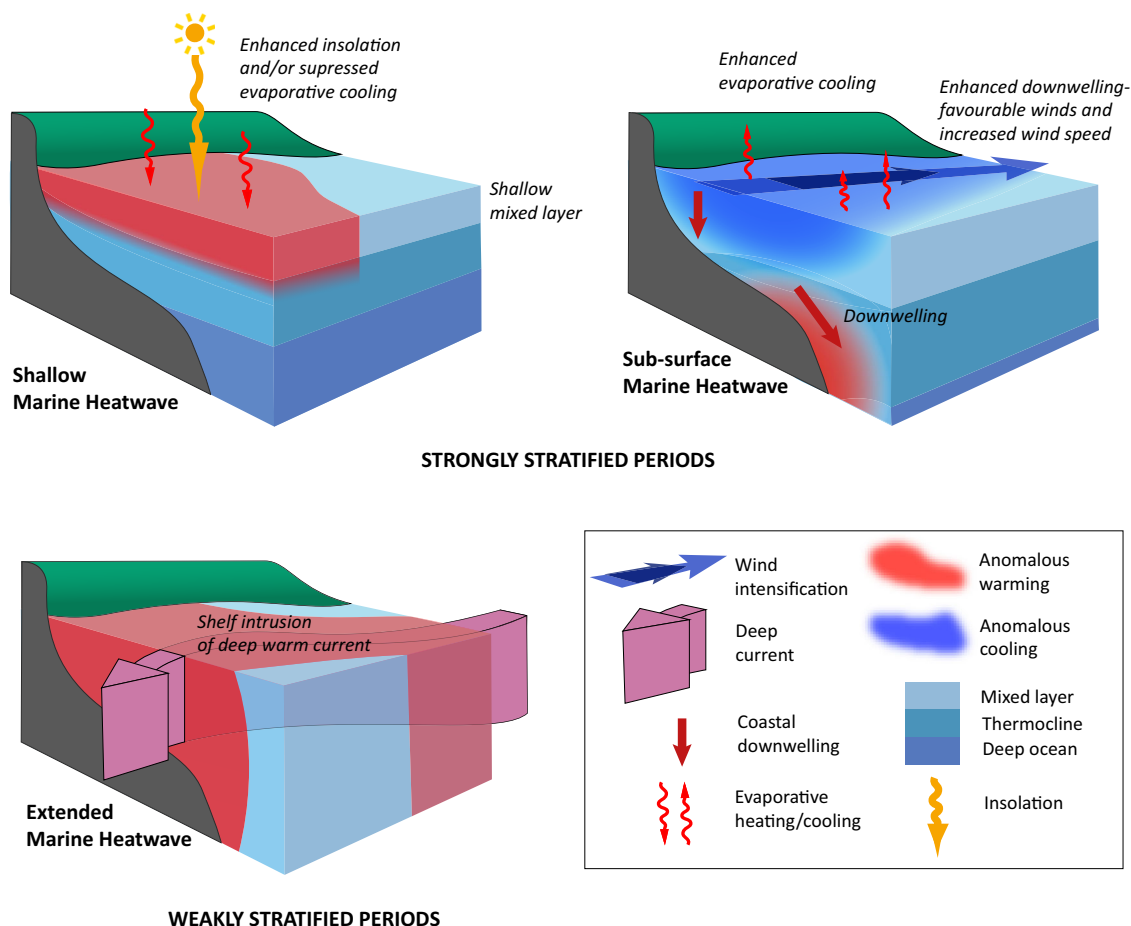
Fig. 8 Schematic of the three MHW classes and related drivers in the region. Characteristics and physical processes affecting *shallow*, *sub-surface*, and *extended* MHWs.

While satellite SST revolutionised our knowledge of temperature extremes, it does not replace deep in situ measurements, and there is a clear need for sustained daily temperature observations below the surface of the ocean to understand processes driving sub-surface MHWs more generally.

Methods

Temperature dataset. Daily temperature measurements were obtained from a mooring off Sydney between 01-Jan-1992 and 31-12-2019 located in 65 m of water at 33.898°S, 151.315°E[35]. The Ocean Reference Station (ORS065[11,28]) is a coastal mooring maintained by Sydney Water. We use hourly temperature data from Aanderaa thermistors at around 0.6, 6.5, 10.5, 14.5, 17, 22.7, 26.1, 29.5, 32.9, 36.3, 39.7, 43.1, 46.5, 49.9 m depths and from a current-meter (InterOcean S4) at 53 m until May 2006. In 2006, the mooring was reconfigured and 13 Aquatech 520T sensors were deployed at 4 m intervals from ~15 m below the surface to 1 m above the seafloor (5 min frequency). All time-series were daily averaged. The individual temperature records at various depths were interpolated over depth into a 1 m vertical grid and binned in 5 m depth intervals from 15 to 50 m. We also kept the deepest record at 53 m. For some analysis, we also include the measurements at 1, 5, and 10 m from 1992 to 2006. The resulting in situ depth bins are 0, 5, 10 m over 1992–2006, and 15, 20, 25, 30, 35, 40, 45, 50, 53 m from 1992 to 2019.

The in situ temperature record was complemented by measurements from satellite SST time-series at the closest pixel at 34°E, 151.4°E (Fig. 1e). We use the climate change initiative (CCI) analysis v2.1 daily gap-free high-resolution (0.05°, 20 cm depth) SST product from the European Spatial Agency (ESA)

until 2016, which has a good correspondence with ARGO compared to many other datasets[36], and is extended between 2016 and 2019 by the Copernicus Climate Change Service (C3S) v2[37]. The comparison of SST at 20 cm depth and 1 m in situ temperature is shown in Supplementary Fig. S1, showing an *r*-square value of 0.93 and a RMSE of 0.6 °C over 1992–2006.

Other dataset. Observed local ocean currents were obtained from a bottom-mounted acoustic Doppler current profiler (ADCP) at the ORS065 mooring site, which provides 5 min estimates of current velocity through the water column at 4 m intervals. We use daily averaged depth-integrated ADCP data from 2007 to 2019 as an estimate of the local ocean circulation. Large-scale ocean current information is provided daily from satellite altimetry (1993–2019, 0.2° resolution), with geostrophic zonal and meridional current velocity. Since satellite altimetry does not resolve the small-scale variability of the shelf circulation[38], we use the time-series from the pixel on the shelf break (34°S, 152°E, Fig. 1f) to represent the mesoscale ocean circulation, including the EAC and eddies. The product is provided by the Integrated Marine Observation System (IMOS) and includes coastal tidal gauge information.

Atmospheric variables from the Australian Bureau of Meteorology (BoM) between 1995 and 2019 are derived from the Sydney airport station (ID 066037, 5 m height, 30 min resolution, at 33.9465°S, 151.1731°E, Fig. 1c). We use daily averages of 2 m air temperature and wind speed and direction to compute the cross-shelf (zonal) and along-shelf (meridional) components of the wind velocity and stress similarly to Wood et al.[39].

Since no observation of air–sea heat fluxes exist in the region, we use 0.25° reanalyses from ERA5 hourly data on single levels[37] from 1992 to 2019. The following variables were extracted at 34.2°S, 151.35°E (Fig. 1c) and daily averaged: mean surface net short-wave and long-wave radiation flux, mean surface latent and sensible heat flux, 10 m u-component and 10 m v-component of wind. A comparison of wind components from BoM Sydney station, ERA5 at ORS065 pixel, and ERA5 at a larger scale (averaged over 150–154°N, 32–36°S) shows good agreement in variability (r-square > 0.85) and magnitude (weak bias) (Supplementary Fig. S2).

All daily anomalies were computed from day-of-the-year moving averages (±5 days) over the whole duration of the datasets (January–December), then smoothed over 31 days (as in ref. [9]): 1992–2019 for satellite and in situ temperature (except for shallow depths, which are only shown for illustration) and ERA5 reanalysis; 1993–2019 for satellite geostrophic currents; 1995–2019 for the BoM meteorological station; 2007–2019 for ADCP current velocities.

MHW identification. MHW identification is done separately for each depth level from the mooring (depth ≥ 15 m) and for the satellite SST. Identification follows the procedure from ref. [9] based on the daily time-series of in situ temperature. A day-of-the-year climatology of the 90th percentile is computed using the maximum time coverage of the mooring dataset (1992–2019) using a moving 10-day window around each day-of-the-year. This climatology is then smoothed (using a 31-day window). MHWs are identified when the temperature exceeds the 90th daily percentile for 5 days or longer, allowing for a 2-day drop below the 90th percentile[9]. MHWs categories (moderate, strong, severe) are also calculated according to Hobday et al.[30]. Note that there is no severe event in the record. This results in a matrix of MHW events over time and depth.

MHW depth-category. For each day over the 1992–2019 period, we investigate the co-occurrence of MHWs across different depths. If 70% or more of the water column depth levels exhibit MHW conditions, we classify this as an *extended MHW*. Events are classified as *shallow MHW* if MHW conditions exist at 0 m from the satellite SST, and 15 m from the in situ observations but MHW conditions are not met at all depths ≥40 m. Conversely, a *sub-surface MHW* occurs when MHW conditions exist at all depths ≥40 m but not at 15 m nor at the surface. The mean intensity, duration and category of events are then extracted from the MHW events at 15, 30 or 53 m, which exhibit a majority of *shallow*, *extended*, or *sub-surface* days, respectively, over the whole duration of the event.

Data availability
ORS065 data is provided by Sydney Water Corporation as a contribution to IMOS and is used under a Creative Commons license (CC BY 4.0). All IMOS data is publicly available and can be found at the Australian Ocean Data Network portal https://portal.aodn.org.au/ or on the server https://thredds.aodn.org.au/thredds/catalog.html. Satellite altimetry dataset was downloaded from https://thredds.aodn.org.au/thredds/catalog/IMOS/OceanCurrent/GSLA/DM/catalog.html. SST data is freely available via the Copernicus Climate Change Service Data Store https://data.marine.copernicus.eu/product/SST_GLO_SST_L4_REP_OBSERVATIONS_010_024/description?view=-&product_id=-&option=-. Atmospheric data from the BoM was obtained through http://www.bom.gov.au/climate/data-services/. ERA5 reanalysis was downloaded from the Copernicus Climate Change Service (C3S) Climate Data Store (Accessed on 08-JUL-2022) https://cds.climate.copernicus.eu/cdsapp#!/dataset/reanalysis-era5-single-levels[31].

Code availability
The MHW detection code was written by Eric C.J. Oliver and available through https://github.com/ecjoliver/marineHeatWaves. Codes used to analyse data and produce figures in this study are available at https://github.com/amandineschaeffer/MHWs_2023_COMMSENV.

References
1. Oliver, E. C. J. et al. Longer and more frequent marine heatwaves over the past century. *Nat. Commun.* **9**, 1324 (2018).
2. Oliver, E. C. J. Mean warming not variability drives marine heatwave trends. *Clim. Dyn.* **53**, 1653–1659 (2019).
3. Frölicher, T. L., Fischer, E. M. & Gruber, N. Marine heatwaves under global warming. *Nature* **560**, 360–364 (2018).
4. Plecha, S. M. & Soares, P. M. M. Global marine heatwave events using the new cmip6 multi-model ensemble: from shortcomings in present climate to future projections. *Environ. Res. Lett.* **15**, 124058 (2020).
5. Qiu, Z., Qiao, F., Jang, C. J., Zhang, L. & Song, Z. Evaluation and projection of global marine heatwaves based on cmip6 models. *Deep Sea Res. Part II: Top. Stud. Oceanogr.* **194**, 104998 (2021).
6. Smale, D. A. et al. Marine heatwaves threaten global biodiversity and the provision of ecosystem services. *Nat. Clim. Change* **9**, 306–312 (2019).
7. Holbrook, N. J. et al. A global assessment of marine heatwaves and their drivers. *Nat. Commun.* **10**, 2624 (2019).
8. Oliver, E. C. et al. Marine heatwaves. *Annu. Rev. Mar. Sci.* **13**, 313–342 (2021).
9. Hobday, A. J. et al. A hierarchical approach to defining marine heatwaves. *Prog. Oceanogr.* **141**, 227–238 (2016).
10. Schlegel, R. W., Oliver, E. C. J., Hobday, A. J. & Smit, A. J. Detecting marine heatwaves with sub-optimal data. *Front. Mar. Sci.* **6**, 737 (2019).
11. Schaeffer, A. & Roughan, M. Subsurface intensification of marine heatwaves off southeastern Australia: the role of stratification and local winds. *Geophys. Res. Lett.* **44**, 5025–5033 (2017).
12. Hu, S. et al. Observed strong subsurface marine heatwaves in the tropical western Pacific Ocean. *Environ. Res. Lett.* **16**, 104024 (2021).
13. Elzahaby, Y. & Schaeffer, A. Observational insight into the subsurface anomalies of marine heatwaves. *Front. Mar. Sci.* **6**, 745 (2019).
14. Rykova, T., Oke, P. R. & Griffin, D. A. A comparison of the structure, properties, and water mass composition of quasi-isotropic eddies in western boundary currents in an eddy-resolving ocean model. *Ocean Model.* **114**, 1–13 (2017).
15. Elzahaby, Y., Schaeffer, A., Roughan, M. & Delaux, S. Oceanic circulation drives the deepest and longest marine heatwaves in the east Australian current system. *Geophys. Res. Lett.* **48**, https://doi.org/10.1029/2021GL094785 (2021).
16. Scannell, H. A., Johnson, G. C., Thompson, L., Lyman, J. M. & Riser, S. C. Subsurface evolution and persistence of marine heatwaves in the northeast pacific. *Geophys. Res. Lett.* **47**, e2020GL090548 (2020).
17. Grosselindemann, H., Ryan, S., Ummenhofer, C. C., Martin, T. & Biastoch, A. Marine heatwaves and their depth structures on the northeast U.S. continental shelf. *Front. Clim.* **4**, 857937 (2022).
18. Amaya, D. et al. Bottom marine heatwaves along the continental shelves of North America. *Nat. Commun.* **14**, 1038 (2023).
19. Smith, K. E. et al. Socioeconomic impacts of marine heatwaves: Global issues and opportunities. *Science* **374**, 6566 (2021).
20. Cook, F. et al. Marine heatwaves in shallow coastal ecosystems are coupled with the atmosphere: Insights from half a century of daily in situ temperature records. *Front. Clim.* **4**, 1012022 (2022).
21. Goebeler, N., Norkko, A. & Norkko, J. Ninety years of coastal monitoring reveals baseline and extreme ocean temperatures are increasing off the Finnish coast. *Commun. Earth Environ.* **3**, 215 (2022).
22. Schlegel, R. W., Oliver, E. C., Wernberg, T. & Smit, A. J. Nearshore and offshore co-occurrence of marine heatwaves and cold-spells. *Prog. Oceanogr.* **151**, 189–205 (2017).
23. Schaeffer, A., Roughan, M. & Morris, B. Cross-shelf dynamics in a western boundary current. implications for upwelling. *J. Phys. Oceanogr.* **43**, 1042–1059 (2013).
24. Ribbat, N., Roughan, M., Powell, B., Rao, S. & Kerry, C. G. Transport variability over the Hawkesbury shelf (31.5–34.5°s) driven by the East Australian current. *PLoS ONE* **15**, e0241622 (2020).
25. Oke, P. R., Pilo, G. S., Ridgway, K., Kiss, A. & Rykova, T. A search for the Tasman front. *J. Mar. Syst.* **199**, 103217 (2019).
26. Sloyan, B. M., Ridgway, K. R. & Cowley, R. The East Australian current and property transport at 27°s from 2012 to 2013. *J. Phys. Oceanogr.* **46**, 993–1008 (2016).
27. Rossi, V., Feng, M., Pattiaratchi, C., Roughan, M. & Waite, A. M. Linking synoptic forcing and local mesoscale processes with biological dynamics off Ningaloo Reef. *J. Geophys. Res.: Oceans* **118**, 1211–1225 (2013).
28. Wood, J. E., Schaeffer, A., Roughan, M. & Tate, P. M. Seasonal variability in the continental shelf waters off southeastern Australia: fact or fiction? *Cont. Shelf Res.* **112**, 92–103 (2016).

29. Schaeffer, A., Roughan, M. & Wood, J. E. Observed bottom boundary layer transport and uplift on the continental shelf adjacent to a western boundary current. *J. Geophys. Res.: Oceans* **119**, 4922–4939 (2014).

30. Hobday, A. et al. Categorizing and naming marine heatwaves. *Oceanography* **31**, (2018). https://tos.org/oceanography/article/categorizing-and-naming-marine-heatwaves.

31. Hersbach, H. et al. *ERA5 hourly data on pressure levels from 1959 to present* (2018) (Copernicus Climate Change Service (C3S) Climate Data Store (CDS), accessed 8 July 2022). https://doi.org/10.1128/ecosalplus.ESP-0015-2019.

32. Hersbach, H. et al. The era5 global reanalysis. *Q. J. R. Meteorol. Soc.* **146**, 1999–2049 (2020).

33. Smit, A. J. et al. A coastal seawater temperature dataset for biogeographical studies: large biases between in situ and remotely-sensed data sets around the coast of South Africa. *PLoS ONE* **8**, e81944 (2013).

34. Benthuysen, J. A., Oliver, E. C. J., Feng, M. & Marshall, A. G. Extreme marine warming across tropical Australia during Austral summer 2015–2016. *J. Geophys. Res.: Oceans* **123**, 1301–1326 (2018).

35. Schaeffer, A., Gramoulle, A., Roughan, M. & Mantovanelli, A. Characterizing frontal eddies along the east Australian current from HF radar observations. *J. Geophys. Res.: Oceans* **122**, 3964–3980 (2017).

36. Beggs, H. Temperature. In *Earth Observation: Data, Processing and Applications*, (eds Harrison, B. A. et al.) Vol. 3B—Surface Waters, Ch 14 (CRCSI, 2021).

37. Merchant, C. J. et al. Satellite-based time-series of sea-surface temperature since 1981 for climate applications. *Sci. Data* **6**, 223 (2019).

38. Schaeffer, A. & Roughan, M. Influence of a western boundary current on shelf dynamics and upwelling from repeat glider deployments. *Geophys. Res. Lett.* **42**, 121–128 (2015).

39. Wood, J. E., Roughan, M. & Tate, P. M. Finding a proxy for wind stress over the coastal ocean. *Mar. Freshw. Res.* **63**, 528–544 (2012).

40. de Boyer Montégut, C., Madec, G., Fischer, A. S., Lazar, A. & Iudicone, D. Mixed layer depth over the global ocean: an examination of profile data and a profile-based climatology. *J. Geophys. Res.: Oceans* **109**, C12003 (2004).

Acknowledgements

Author contributions

A.S. conceived, designed, performed the analysis and wrote the paper; A.S.G. and M.R. contributed to the design and writing; A.S.G. created Fig. 8; M.R. contributed to the data collection.

Competing interests

The authors declare no competing interests.

Additional information

Supplementary information The online version contains supplementary material available at https://doi.org/10.1038/s43247-023-00966-4.

Correspondence and requests for materials should be addressed to Amandine Schaeffer.

Peer review information *Communications Earth & Environment* thanks Robert Schlegel and the other, anonymous, reviewer(s) for their contribution to the peer review of this work. Primary Handling Editors: Regina Rodrigues, Heike Langenberg. A peer review file is available.

Reprints and permission information is available at http://www.nature.com/reprints

Publisher's note Springer Nature remains neutral with regard to jurisdictional claims in published maps and institutional affiliations.